Eur. Phys. J. B **2**, 301–311 (1998)

THE EUROPEAN PHYSICAL JOURNAL B

Contributions to photodoping in oxygen-deficient $YBa_2Cu_3O_x$ films

C. Stockinger[1,a], W. Markowitsch[1], W. Lang[1], W. Kula[2], and R. Sobolewski[2,b]

[1] Institut für Materialphysik, Universität Wien and Ludwig Boltzmann Institut für Festkörperphysik, Kopernikusgasse 15, 1060 Wien, Austria
[2] Department of Electrical Engineering and Laboratory of Laser Energetics, University of Rochester, Rochester, NY 14627, USA

Received: 13 October 1997 / Accepted: 19 November 1997

Abstract. We report our studies on the superconducting and normal-state properties of metallic $YBa_2Cu_3O_x$ thin films ($T_{c,mid} \approx 52$ K) exposed to long-term white-light illumination (photodoping). It was observed that the effects of photoexcitation strongly depended on the temperature at which the photodoping was performed. At low temperatures, both the Hall mobility and the Hall number were photoenhanced, whereas, at temperatures slightly below room temperature, the Hall mobility initially showed an abrupt increase followed by a long-term decrease, and the Hall number increased even stronger than at low temperatures. The enhancement of the film's superconducting transition temperature T_c, caused by photodoping, exhibited the same temperature dependence as the enhancement of the Hall number, being largest ($\Delta T_c \approx 2.6$ K) at high temperatures. From the asynchronous behavior of the Hall quantities, we conclude that both the photoassisted oxygen ordering and charge transfer mechanisms contribute to photodoping. The relative contributions of both mechanisms and, thus, the electronic properties of the photoexcited state are strongly temperature dependent. Studies of the relaxation of the photoexcited state at 290 K showed an unexpectedly short relaxation time of the Hall mobility after termination of the illumination. The relaxation saturated somewhat below the initial, undoped value, similarly to the decrease of the Hall mobility, observed upon long illumination. These latter findings give evidence for a competition between the oxygen ordering and thermal disordering processes during and after the photoexcitation in the high-temperature range.

PACS. 73.50.Jt Galvanomagnetic and other magnetotransport effects (including thermomagnetic effects) – 73.50.Pz Photoconduction and photovoltaic effects – 74.76.Bz High-T_c films

1 Introduction

Various experiments have shown that physical properties of $YBa_2Cu_3O_x$ (YBCO) compounds with nominal oxygen concentrations in the $6 < x < 7$ range are changed persistently by long-term illumination with white light or visible laser radiation [1–14]. It has been shown that this remarkable phenomenon, known as persistent photoconductivity (PPC), is a common feature of all oxygen-deficient YBCO samples. In samples with $x \approx 6.4$, prolonged illumination progressively transforms YBCO from a semiconducting (nonsuperconducting) state to a metallic state that exhibits a superconducting transition at low temperatures [1–3]. In the superconducting samples ($6.4 < x < 7$), the illumination causes not only a decrease of the electrical resistivity, but also a simultaneous increase of the superconducting transition temperature T_c [4–8]. A light-induced change of the Hall coefficient and the Hall mobility was observed in oxygen-deficient YBCO [5–7,9]. Furthermore, an increase of the orthorhombicity of the crystal structure was concluded from a contraction of the c-axis lattice parameter [10,11]. Additional evidence for photoinduced structural modifications was provided by the observation of an increase of the superconducting coherence lengths ξ_{ab} and ξ_c [12]. A measurable decay of the photoexcited state was observed only at temperatures above 250 K in metallic YBCO [13] and above 270 K in insulating YBCO [3,14]; below these temperatures the PPC was found to be indeed persistent.

Attempts to clearly observe PPC in other high-temperature superconducting (HTS) materials have failed. Osquiguil *et al.* [7] did not observe PPC in $Bi_2Sr_2CaCu_2O_{8-x}$ and $La_{2-y}Sr_yCuO_{4-x}$, and Tanabe *et al.* [15] reported even an increase of the resistivity in $Bi_2Sr_2CaCu_2O_{8-x}$ caused by illumination. The latter effect showed no relaxation at room temperature. Very recently Szymczak *et al.* [16] showed the existence of

[a] e-mail: stock@pap.univie.ac.at
[b] Also at the Institute of Physics, Academy of Sciences, 02668 Warszawa, Poland.

persistent photoinduced effects in $Tl_2Ba_2CaCu_2O_8$ superconducting thin films. Both the intrinsic (T_c enhancement) and extrinsic (magnetic properties) effects were observed, but the explanation was based on two different types of photosensitive pinning centers in the Tl-based compound.

The aforementioned results suggest that PPC is strongly correlated to the oxygen stoichiometry of YBCO. The unit cell of the $x = 7$ compound contains CuO_2 double planes and CuO chains, the latter playing the role of charge carrier reservoirs for the planes [17]. It is well known that the chain oxygen ions are weakly bounded and can be easily removed by temperature treatments in oxygen-poor atmospheres [18,19]. Near $x = 6.5$ the chains seem to be partially ordered in what is sometimes called the ortho-II phase [20], but, in general, the CuO chains in partially oxygen-deficient samples consist of more or less disordered segments.

All proposed models for PPC in YBCO are based on a specific defect structure within the CuO chains. In the so-called *charge transfer* model, developed by Kudinov *et al.* [3], sample illumination generates electron-hole pairs in the CuO_2 planes. Subsequently, electrons are transferred to the CuO chains and trapped there in unoccupied p-levels of oxygen ions, while holes remain mobile in the planes. The trapped electrons induce a local potential distortion resulting in an energy barrier of about 1 eV [3,14] that, at low temperatures, prevents the recombination of the electrons with the excess holes, resulting in PPC. Hence, the persistent increase of conductivity, T_c enhancement, and the semiconductor-to-metal transition can be naturally explained by the *charge transfer* model. In addition, the model can account for the wavelength dependence of PPC, predicting the onset of the photodoping efficiency [3,21,22] at the *charge transfer* gap energy (approximately 1.6 eV) of the semiconducting YBCO [23]. On the other hand, the *charge transfer* model has difficulty describing the c-axis shrinking and the increase of the Hall mobility during the photoexcitation.

The *photoassisted oxygen-ordering* model, proposed by Nieva *et al.* [5], was stimulated by the apparent similarity of PPC to the effect of room-temperature aging in YBCO samples quenched down from high annealing temperatures [24]. The authors argued that since the activation energy of the chain-oxygen ions is close to 1.2 eV [6,25], visible light photons used in PPC experiments should be able not only to excite electron-hole pairs, but first of all to induce movements of the oxygen ions and, thereby, enable oxygen reordering in a way that the average length of the CuO chain increases. It is well known that the increased length of the CuO chains results in an increase of the free carrier (hole) concentration within the CuO_2 planes. Obviously, the *oxygen-ordering* model is able to explain a variety of PPC-related structural changes in YBCO crystals.

The situation became more complicated when Hasen *et al.* [26] presented their experimental results on oxygen-poor ($x \approx 6.3$) YBCO samples. The authors observed that a relative enhancement of the photoinduced conductivity in their samples increased with the decreasing of x. This was in direct disagreement with the predictions of both the *charge transfer* and *oxygen-ordering* models since in the region of very low oxygen contents the number of oxygen ions should be too small to either act as trapping centers for the photoexcited electrons, or form CuO chains of sufficient lengths. Following an earlier suggestion made by Kreines and Kudinov [27], Hasen *et al.* [26] introduced the *oxygen vacancy capture* model. In this model, the photoexcited electrons are trapped by oxygen vacancies in the CuO chains, in analogy to the DX-centers in GaAs (in our opinion, this should read "F-centers"). Since the number of oxygen vacancies increases with decreasing x, the relative photoinduced conductivity enhancement is expected to show the observed increasing tendency. The *vacancy capture* model has, however, the same limitations as the *charge transfer* model in explaining the YBCO structural changes during the photodoping.

We want to stress that each of the above discussed models uses the same initiating process, *i.e.*, the generation of electron-hole pairs within the CuO_2 planes. The *vacancy capture* and *charge transfer* mechanisms are physically quite similar since they differ "only" in the nature of the trapping centers. On the one hand, the main difference between these two mechanisms and the *photoassisted oxygen ordering* is that the latter involves an additional step, namely the light-induced ordering of oxygen ions. Considering a disordered structure of the oxygen-deficient YBCO, where the presence of unoccupied p-levels, oxygen vacancies, and a certain, disordered arrangement of chain segments can be expected, it seems quite reasonable that all of the above processes may simultaneously contribute to PPC. The proportion of the contributions, however, should depend on the oxygen content x and on the temperature at which the photodoping is performed.

The aim of this paper is to present *in situ* studies of the time evolution of the transport properties of partially oxygen-depleted epitaxial YBCO thin-film samples, light illuminated at different temperatures, and to determine the exact role and contribution of each of PPC mechanisms in the photodoping process. In our previous paper [28], we used the *in situ* Hall effect and resistivity measurements to discriminate between different physical mechanisms contributing to PPC. We observed markedly different time evolution of the Hall coefficient and the Hall mobility during long-term illumination of metallic YBCO films. Our conclusion was that several mechanisms participate in the photodoping process. Here, we extend these preliminary studies by including different doping temperatures and giving a comprehensive description of the effects of prolonged light illumination on the transport properties of YBCO, including the resistance, Hall resistivity, and T_c. In addition, we investigate the relaxation of PPC at 290 K and during the PPC "erasing" procedure, performed at 310 K. The presented results indicate that not only the effectiveness of photodoping, but also the electronic properties of the photodoped state are strongly dependent on the temperature at which the photodoping process is conducted. In particular, we find an evidence for a direct competition between oxygen *ordering* and *disordering* processes near room temperature. These

structural instabilities directly influence the carrier mobility, but, at the same time, seem to have only an indirect influence on the free carrier concentration in the material. Our paper is organized as follows. In Section 2, we describe the sample preparation and the experimental techniques, stressing accuracy and reproducibility of our measurement method. In Section 3, we present our experimental results on photodoping, T_c enhancement, and PPC relaxation. In Section 4, the data analysis with regard to the existing models of PPC is discussed. Finally, in Section 5, we conclude our findings and comment on some implications coming from our results.

2 Sample preparations and measurement methods

Samples used in our experiments were about 140-nm-thick YBCO films deposited *in situ* by rf sputtering on $LaAlO_3$ substrates. As-deposited films were fully oxygenated and exhibited a 0.5-K-wide superconducting transition at approximately 90 K. Subsequently, the oxygen content of our films was reduced by annealing for 1 to 2 h at 330 °C to 450 °C in 20 mTorr of oxygen and cooling down to 270 °C within 20 min, followed by a quench to room temperature. Depending on the annealing temperature, T_c values from 10 K to 80 K were obtained with this method [29]. The reversibility of the process was checked by re-oxidizing some of the previously oxygen-depleted films. Within 1 K to 2 K, the initial T_c value was reproduced, showing that the annealing procedure did not degenerate our films or change their structural integrity. For the presented studies, samples belonging to the so-called "60-K plateau" of YBCO were used. The $T_{c,mid}$ was about 52 K, applying the midpoint-of-transition criterion. According to reference [7], this corresponds to an oxygen content of $x \approx 6.5$ to 6.6. Test structures were patterned by a laser inhibition technique [30], allowing measurement of the resistivity and the Hall voltage in the usual 6-point geometry.

In situ measurements of the resistivity and the Hall effect during the light illumination and PPC relaxation were performed in a temperature-controlled closed-cycle refrigerator, with the sample mounted on a cold finger. The sample was illuminated through a Suprasil glass window with a quartz tungsten halogen lamp. An estimated light intensity of 1 W/cm^2 on the surface of the sample was used for the illumination. A water filter was placed in the optical path to eliminate the infrared part of the radiation. Long-term temperature stability was substantially improved, compared with our previous studies reported in reference [28], by (a) applying an additional inner heat shield around the sample with an entrance slit of about 1 cm^2; and (b) mounting the temperature sensor close to the sample and illuminating it together with the sample. With these measures, the initial temperature rise after turning on the lamp was limited to ≤ 0.5 K and within a few minutes was completely nullified by the temperature control system.

For the Hall-effect measurements, an electromagnet provided a magnetic field of $B = 0.52$ T perpendicular to the film's surface. The electrical measurements were performed with a lock-in technique and a very stable 17 Hz current source. The experimental setup was fully computer controlled. Both the longitudinal and Hall voltages in both polarities of the magnetic field and at the zero field were recorded during the experiment at every 1.4 min. For the relaxation measurements, the Suprasil window in the cryostat was covered with an Al foil to rule out any influence of daylight or other stray radiation.

The following measurement procedure was implemented. After an initial cool-down from 310 K to 40 K to determine the YBCO's intrinsic T_c, the temperature was raised to a desired experimental temperature T and the sample was photodoped for time t of 48 h. Next, it was immediately cooled down again to determine the T_c enhancement. Finally, the film was warmed up to 310 K and kept there for 24 h to allow a complete decay of PPC. Later, the cycle was repeated, including the initial cool-down to check reproducibility of our measurements, with the photodoping carried out at a different temperature. The experimental setup was kept absolutely unchanged during the entire sequence of measurements, which lasted for several weeks, so the measurements performed at different doping temperatures could be really comparable.

3 Experimental results

3.1 Photodoping experiments

Figure 1 shows the longitudinal resistivity $\rho_{xx}(t)$, measured during white-light illumination for 48 h at 70 K, 100 K, 200 K, 260 K, and 290 K, normalized to its starting value $\rho_{xx}(0)$ at $t = 0$, respectively. The light intensity and, thus, the cumulative photon dose were the same in each of the measurements. At the beginning, $\rho_{xx}(t)/\rho_{xx}(0)$ dropped rapidly, followed by a slower decrease at long illumination times. At $t < 2$ h, the differences between the data collected at different temperatures were small, but at longer times the curves split up and the total reduction of the resistivity achieved after 48 h (we will call this value the photodoping effectiveness) strongly depended on the temperature. The effectiveness was largest at 260 K (about 13%), and smallest at 200 K (about 9%). At the other studied temperatures, the values of effectiveness of about 10% to 11% were observed. Up to 260 K there is no sign of saturation of the $\rho_{xx}(t)/\rho_{xx}(0)$ function, in agreement with our previous results [28]. The lack of saturation is clearly visible in the inset in Figure 1, where $\rho_{xx}(t)/\rho_{xx}(0)$ is plotted in the logarithmic time scale.

Figure 2 shows the normalized Hall resistivity $\rho_{yx}(t)/\rho_{yx}(0)$ as a function of the illumination time at the studied temperatures. Compared with $\rho_{xx}(t)/\rho_{xx}(0)$, $\rho_{yx}(t)/\rho_{yx}(0)$ displayed a quite different behavior of the effectiveness of photodoping. At temperatures up to 200 K, the effectiveness of only 5% to 6% was achieved, whereas at both 260 K and 290 K, it sharply increased to about 11%. We note that at temperatures up to 260 K, $\rho_{xx}(t)/\rho_{xx}(0) > \rho_{yx}(t)/\rho_{yx}(0)$ at $t = 48$ h, and

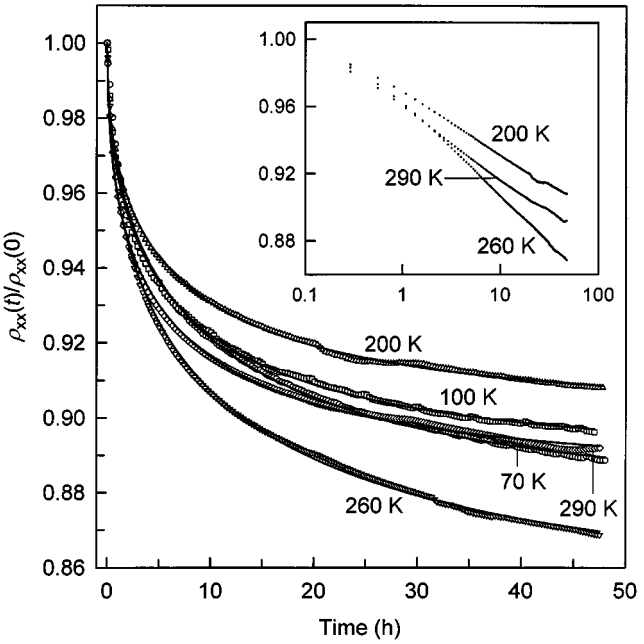

Fig. 1. Time dependence of the normalized longitudinal resistivity $\rho_{xx}(t)/\rho_{xx}(0)$ of $YBa_2Cu_3O_x$ ($x \approx 6.5$) during white-light illumination, measured at the indicated temperatures. Solid lines represent the fits obtained with the help of equation (1). The inset shows three of the data curves plotted on a logarithmic time scale.

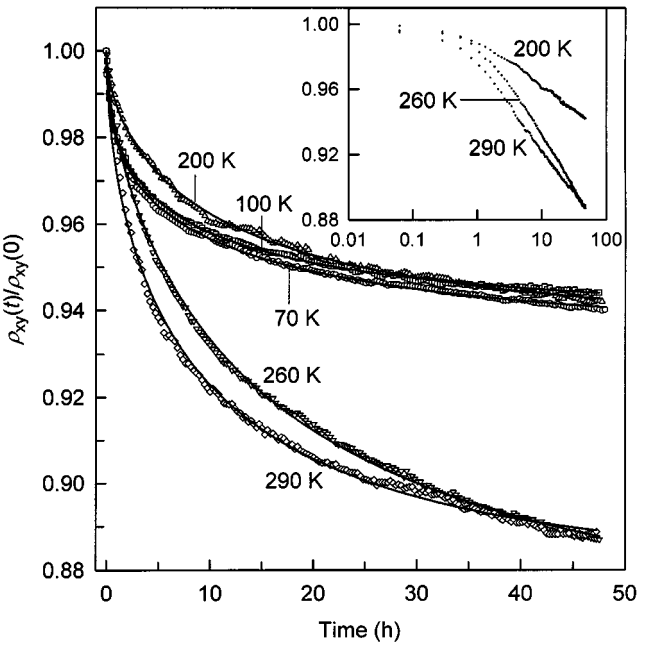

Fig. 2. Time dependence of the normalized Hall resistivity $\rho_{yx}(t)/\rho_{yx}(0)$ of $YBa_2Cu_3O_x$ ($x \approx 6.5$) in a magnetic field of $B = 0.52$ T, measured under the same conditions as $\rho_{xx}(t)/\rho_{xx}(0)$ in Figure 1. Solid lines represent the fits obtained with the help of equation (1). The inset shows three of the data curves plotted on a logarithmic time scale.

only at 290 K does the opposite relation hold. Similarly to $\rho_{xx}(t)/\rho_{xx}(0)$, no saturation was observed in the $\rho_{yx}(t)/\rho_{yx}(0)$ dependence (see inset in Fig. 2).

The time dependences of $\rho_{xx}(t)$ and $\rho_{yx}(t)$ are clearly nonexponential. In agreement with previous results [13,28], the experimental data can be well described by the empirical stretched-exponential Kohlrausch expression [3]:

$$\rho_{ik}(t) = \rho_{ik}(t \to \infty) + [\rho_{ik}(0) - \rho_{ik}(t \to \infty)] \exp\left\{-(t/\tau_{ik})^{\beta_{ik}}\right\}, \quad (1)$$

where ik is replaced by either xx or yx depending on the quantity under consideration. $\rho_{ik}(t \to \infty)$ is the saturation value of $\rho_{ik}(t)$, τ_{ik} is a time constant, and β_{ik} is a dispersion parameter ($0 < \beta_{ik} < 1$). The solid lines in Figures 1 and 2 show equation (1) fits to the experimental data. The agreement is very good, although, as reported previously [13], at large illumination times the measured values show a general tendency to fall somewhat below the theoretical curves. We note that we observed no systematic dependence on the temperature in Figure 1, in contrast to the results of relaxation measurements [3,13]. The most probable reason for this discrepancy is the surprizingly different behaviors of the Hall number and the Hall mobility during illumination (see below).

To separate the different contributions to the photodoping effect, the Hall number $p_H = 1/R_H e$ ($R_H = \rho_{yx}/B$ is the Hall coefficient) and the Hall mobility $\mu_H = R_H/\rho_{xx}$ were calculated from $\rho_{xx}(t)$ and $\rho_{yx}(t)$. Theoretical difficulties associated with the Hall effect interpretation in YBCO will be discussed in Section 4 — here we only want to point out that within a single-band model, changes of p_H and μ_H can be considered to reflect changes of the free hole concentration and the hole mobility in YBCO films, respectively. In Figure 3, it is shown that p_H increases strictly monotonously as a function of time at all studied temperatures, and even after 48 h of illumination there is no sign of a saturation in any of the curves. Interestingly, the enhancement of p_H is almost the same at 260 K and 290 K, so one must conclude that the different effectivenesses observed earlier in ρ_{xx} must arise from the temperature dependence of the Hall mobility. We also note that, for times below 30 h of illumination time, the increase of p_H is largest at 290 K but shows a flattening dependence at larger times. We take this latter effect as a sign of PPC relaxation, which becomes important in this temperature and time range.

As compared to p_H, the Hall mobility $\mu_H(t)$ displays a remarkably different behavior, shown in Figure 4. At 70 K and 100 K, $\mu_H(t)$ shows a very similar functional dependence as $p_H(t)$, *i.e.*, a monotonical increase without a saturation up to 48 h of illumination. However, the time dependence of μ_H changes dramatically when the photodoping temperature is increased. At 200 K, $\mu_H(t)$ saturates after approximately 18 h of illumination, while at higher temperatures, $\mu_H(t)$ *decreases* at large illumination times. At both 260 K and 290 K, $\mu_H(t)$ increases at the very beginning of the photodoping process, reaches a maximum value after a few hours of illumination, and subsequently decreases. It is obvious from Figure 4 that

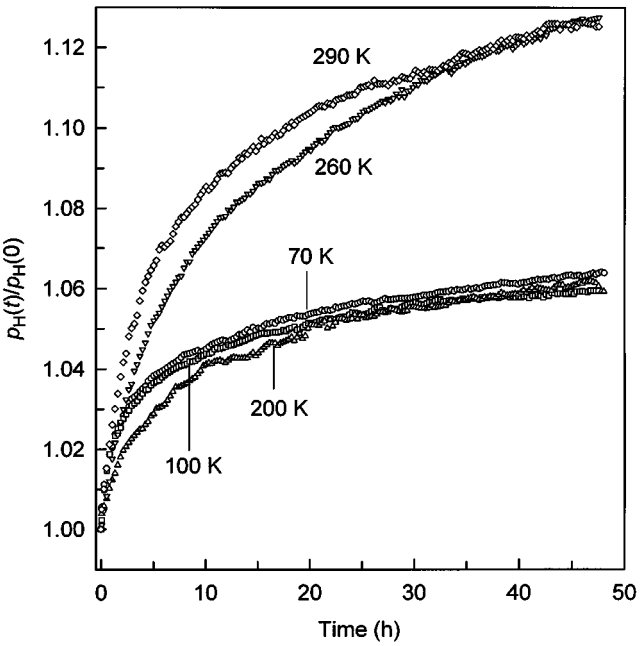

Fig. 3. Normalized Hall number $p_H = 1/R_H e$ as a function of the illumination time, taken at the indicated temperatures.

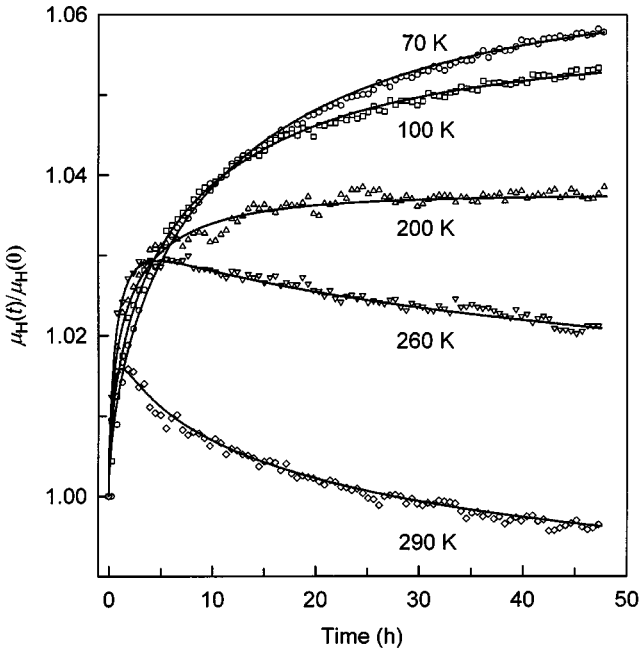

Fig. 4. Normalized Hall mobility $\mu_H = R_H/\rho_{xx}$ as a function of the illumination time, taken at the indicated temperatures. Solid lines are fits to the data by the average of two Kohlrausch terms, one increasing and the other decreasing as a function of time.

the process responsible for the mobility enhancement at low temperatures is still present at higher temperatures, but it is counteracted by another process showing a falling tendency. It should be noted that, in contrast to p_H (48 h), μ_H (48 h) shows a monotonical temperature dependence and that at 290 K, μ_H (48 h) is somewhat *smaller* than the original, undoped value. The observed behavior con-

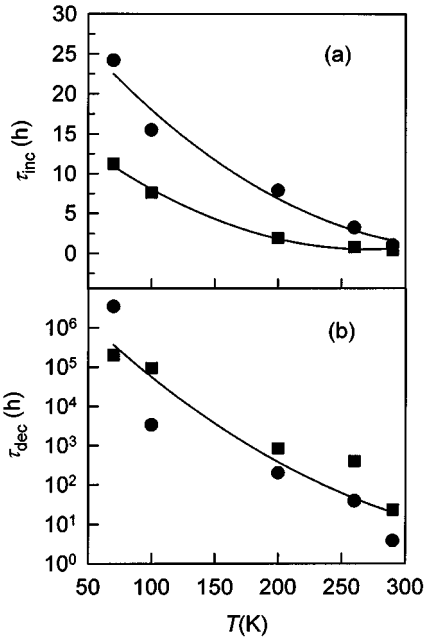

Fig. 5. The time constants of (a) the increasing part τ_{inc} and (b) the decreasing part τ_{dec} of the Hall mobility shown in Figure 4, plotted as a function of temperature. The squares denote the results from "model 1", the circles from "model 2" (see text). In "model 2", the fit parameters were $\mu_{max}/\mu_H(0) = 1.158$, $\mu_{min}/\mu_H(0) = 0.828$, and $\beta_{inc} = \beta_{dec} = 0.464$. Solid lines are guides to the eye.

firms our previous results [28] but is considerably different from the results presented by other groups. The other published data show only a monotonical increase of the Hall mobility during the illumination [6,9] with the exception of a remark made by Osquiguil *et al.* [7], who stated (without showing an appropriate figure) that in a sample with the oxygen content $x = 6.7$, μ_H decreased during the photodoping at room temperature.

To better understand the temperature dependence of μ_H, we fitted the data in Figure 4 to stretched exponential functions similar to equation (1) (solid lines in Fig. 4). At 200 K, 260 K, and 290 K, the experimental curves can be well fitted by the arithmetical average of two Kohlrausch terms $\mu_H/\mu_H(0) = (\mu_{inc} + \mu_{dec})/2\mu_H(0)$, where μ_{inc} increases and μ_{dec} decreases with the illumination time. We find that both $\mu_{max}/\mu_H(0) = \mu_{inc}(t \to \infty)/\mu_H(0)$ and $\mu_{min}/\mu_H(0) = \mu_{dec}(t \to \infty)/\mu_H(0)$ decrease with increasing temperature ($\mu_{min}/\mu_H(0) = 0.99$ at 200 K). At the low temperatures, μ_{dec} is not unambiguously defined by the data, especially when all six free parameters are used for the fits. We focused our attention on the temperature dependences of the time constants τ_{inc} and τ_{dec}, used to characterize the increasing and decreasing Kohlrausch terms at all temperatures, and reduced the number of free parameters making several assumptions. In a first model ("model 1"), we assumed $\beta_{dec} = 0.5$ at all temperatures and $\mu_{min}/\mu_H(0) = 0.99$ between 70 K and 200 K and found that $\mu_{max}/\mu_H(0)$ decreased from 1.13 at 70 K to 1.06 at 290 K. In a second, simplified model

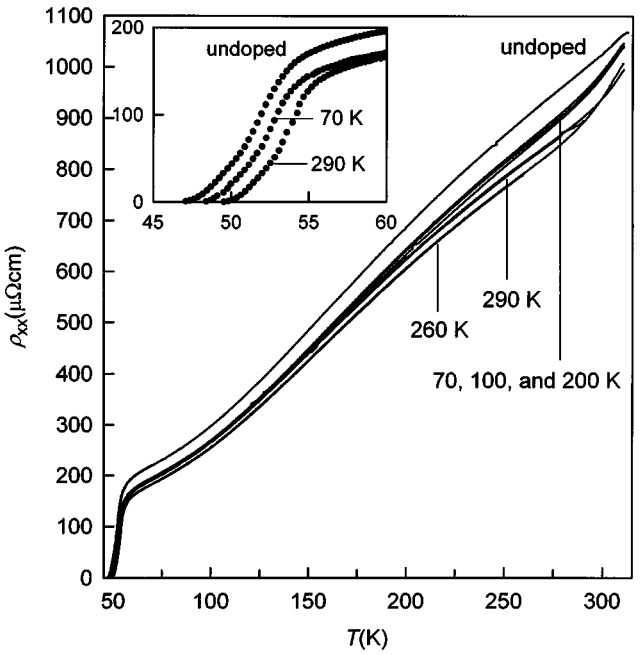

Fig. 6. The $\rho_{xx}(T)$ characteristics measured after each of the photodoping sessions, carried out with identical photon doses at the indicated temperatures. The inset shows the superconducting transition region on an enlarged temperature scale (for clarity, only three of the curves are plotted).

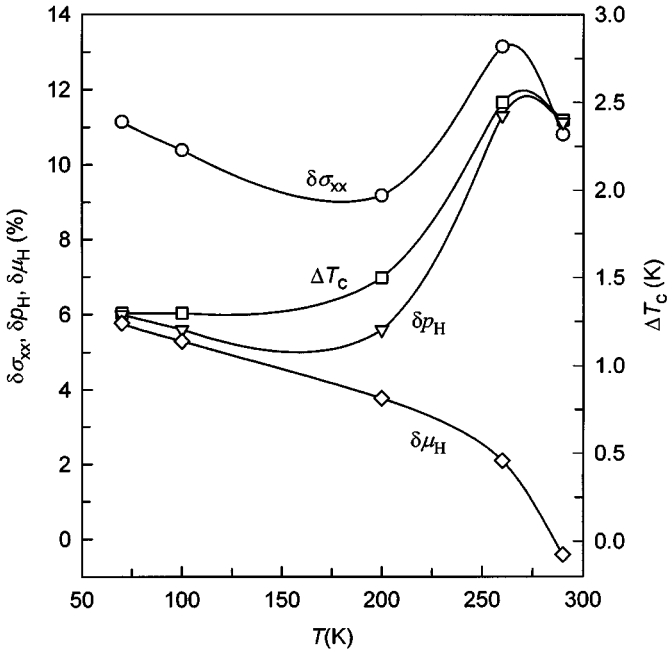

Fig. 7. Relative changes of the longitudinal conductivity $\delta\sigma_{xx}$, the Hall number δp_H, the Hall mobility $\delta\mu_H$, and the absolute T_c enhancement ΔT_c, after light excitation for 48 h, plotted as a function of the photodoping temperature. Solid lines are just guides to the eye.

("model 2"), we assumed that $\mu_{max} = \mu_{inc}(t \to \infty)$ and $\mu_{min} = \mu_{dec}(t \to \infty)$ are temperature independent, and that $\beta_{inc} = \beta_{dec}$. Figure 5a shows that in both scenarios, τ_{inc} decreases roughly linearly with increasing temperature, changing by about one order of magnitude, whereas τ_{dec} decreases approximately exponentially by several orders of magnitudes (Fig. 5b). From these findings, we conclude that the kinetics of $\mu_H(t)$ is accelerated by increasing the temperature.

Finally, we want to point out that the lack of a systematic behavior of $\rho_{xx}(t)$ is simply a consequence of the dependences of $p_H(t)$ and $\mu_H(t)$ (Figs. 3 and 4, respectively). In $\rho_{xx}(t)$ $(= 1/p_H\mu_H e)$ these two considerably different dependences on temperature are mixed, resulting in an apparent non-systematic behavior of $\rho_{xx}(t)$.

3.2 T_c enhancement

As described in Section 2, the T_c of our samples was measured before and after each of the photodoping experiments. Figure 6 presents the $\rho_{xx}(T)$ characteristics measured for an undoped film and after the photodoping at every studied temperature. It should be pointed out that the curves measured for the "erased" samples always overlaid, within the accuracy of our measurement, the characteristics obtained for an undoped, nonilluminated sample. We observe in Figure 6 that the $\rho_{xx}(T)$ curves of the samples photodoped up to 200 K overlay each other and are more or less shifted parallel with respect to the undoped curve. Above 200 K, the $\rho_{xx}(T)$ characteristics show measurable shape differences, depending strongly on the doping temperature. The curves collected at the 260 K and 290 K doping temperatures exhibit substantially lower resistivity values and intersect at 290 K. In addition, near room temperature, all of our curves show a pronounced increase toward the $\rho_{xx}(T)$ dependence of the nonilluminated sample. The obvious reason for this latter observation is that the duration of our measurement becomes comparable to the PPC relaxation time. Our previous results [12] showed that, at about 320 K, the characteristics of photodoped samples collapsed with the undoped one. Based on the data presented in Figure 6, we have to conclude that photodoping carried out at different temperatures but with identical photon doses leads to different $\rho_{xx}(T)$ characteristics and, hence, to photoexcited states of the different electronic structure. This result is in agreement with our observations based on the photodoping experiments discussed in Section 3.1. The inset in Figure 6 shows the superconducting transition regions of three of the curves in more detail. We observe that not only the value of T_c has increased upon illumination, but also the width and the shape of the transition changed slightly with temperature. If we define the T_c enhancement ΔT_c as the shift of the offset temperature (*i.e.*, where $\rho_{xx}(T) = 0$), we find that ΔT_c depends strongly on the temperature at which the photodoping was performed.

Photodoping at temperatures up to 200 K resulted in $\Delta T_c \approx 1.3$ K, but at 260 K and 290 K, ΔT_c was approximately twice as large (see inset in Fig. 6). This final result is of particular importance since the value of T_c is correlated to the carrier concentration in the material [31].

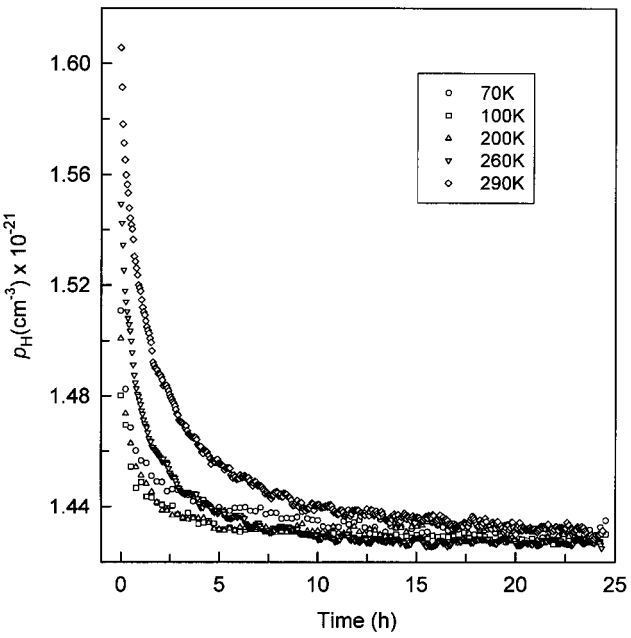

Fig. 8. Time dependence of the Hall number during relaxation at 310 K after photodoping at the temperature indicated in the figure.

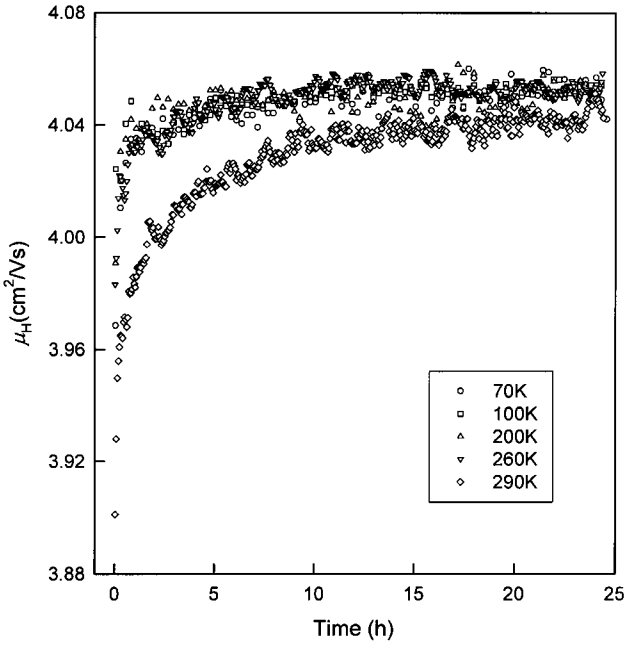

Fig. 9. Time dependence of the Hall mobility during relaxation at 310 K after photodoping at the temperature indicated in the figure.

Figure 7 gives a summary of discussed in Sections 3.1 and 3.2 effects of photodoping in our YBCO samples. The relative changes $\delta\sigma_{xx}$, δp_H, and $\delta\mu_H$ of $\sigma_{xx} = 1/\rho_{xx}$, p_H, and μ_H are expressed as the percentage of the corresponding initial values, respectively, and are plotted together with ΔT_c. As can be clearly seen in Figure 7, ΔT_c depends on the photodoping temperature essentially in the same way as δp_H, what confirms that the enhancement of both these quantities is governed by the enhancement of the same electronic parameter, *i.e.*, the free-carrier concentration. In obvious contrast, $\delta\sigma_{xx}$ and $\delta\mu_H$ show completely different temperature dependences, due to the complicated behavior of μ_H during the illumination process (see Fig. 4).

3.3 PPC relaxation

During the experimental session (see Sect. 2), PPC was always erased between every two photodoping measurements. For this purpose, after the termination of illumination and the T_c measurement, the sample was warmed up to 310 K and held there for 24 h. During the PPC relaxation at 310 K, ρ_{xx} and ρ_{yx} were monitored every 1.4 min. From the data, the time dependences $p_H(t)$ (Fig. 8) and $\mu_H(t)$ (Fig. 9) were calculated the same way as for Figures 3 and 4. Due to different values at the end of the photodoping process, the relaxation curves start at different onsets, but they ultimately reach the same saturation values $p_H(310\ \mathrm{K}) = 1.43 \times 10^{21}\ \mathrm{cm}^{-3}$ and $\mu_H(310\ \mathrm{K}) = 4.05\ \mathrm{cm}^2/\mathrm{Vs}$ within $< 0.5\%$. These results confirm that our PPC erasing procedure worked well and reproducibly. It should be noted that the shapes of the $p_H(t)$ and $\mu_H(t)$ relaxation curves depended on the temperature at which the preceding photodoping was carried out. The full assessment of the data presented in Figures 8 and 9 must consider the structural changes occurring in YBCO annealed near room temperature. Kawamoto and Hirabayashi [10] observed in an insulating sample that after heating up from 295 K to 314 K the resistance showed a pronounced relaxation behavior for several hours. In our partially oxygen-depleted samples, we may expect a similar effect after warming up to 310 K.

The influence of temperature-induced structural changes during the PPC relaxation process is even more evident from a comparative study of p_H and μ_H. Figure 8 shows that p_H relaxes, as expected, from the photoenhanced value to its initial undoped state. In contrast, μ_H (Fig. 9) exhibits an *increase* after *all* photodoping experiments, regardless of its behavior during the photodoping process itself (Fig. 4). This result can be understood only if the photoenhancement of μ_H, observed at low temperatures, was lost during the warm-up period to the 310 K level. Thus, we can conclude that μ_H relaxation at 310 K is mainly caused by structural changes in our oxygen-deficient YBCO samples induced by the temperature sweep and should not be compared to photodoping.

To further prove the above statement, we performed a separate photodoping/relaxation experiment at a constant temperature of 290 K. A YBCO sample was photodoped for 24 h, then the illumination was terminated and the relaxation of the photodoped state was followed for another 48 h. Figure 10 shows p_H and μ_H dependences on time during the entire experiment. We note that the photodoping part of this experiment is in excellent agreement with the previous results presented in Figures 3 and 4. As before, p_H increased until the illumination was terminated

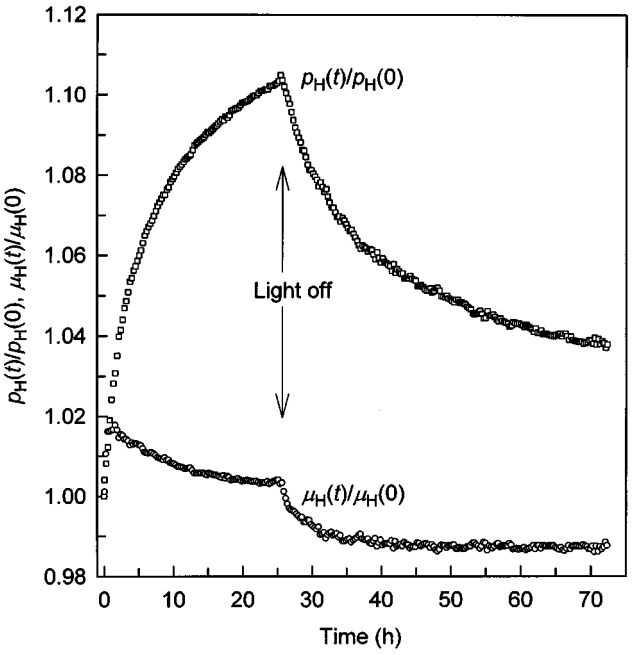

Fig. 10. Normalized Hall number $p_H(t)/p_H(0)$ and Hall mobility $\mu_H(t)/\mu_H(0)$ during illumination for 24 h, followed by the relaxation of the photodoped state for additional 48 h. The arrows indicate the termination of illumination.

and μ_H showed the initial fast increase followed by a slow long-term decrease. After the termination of the photoexcitation, μ_H dropped rapidly and within about 15 h reached a constant, saturation value, while p_H relaxed far more slowly and, even after 48 h, the initial value had not been reached. It should be also noted that μ_H relaxed to a saturation value, which was somewhat *below* the initial, undoped one. This finding corresponds to Figure 4, where μ_H, during the photodoping at 290 K, also decreased below its initial value. Unfortunately, the accuracy of our measurement is not sufficient to decide whether at 290 K μ_H shows a trend to return (rise) to its undoped value after longer than 48 h relaxation, as it happened during relaxation at 310 K.

Numerical fits (not shown) of the relaxation data presented in Figure 10, based on the stretched-exponential law similar to equation (1), yielded relaxation times of 14.6 h and 4.2 h for p_H and μ_H, respectively. From our earlier PPC relaxation studies [13], we expect a factor of 10 decrease in relaxation time when the temperature is increased from 290 K to 310 K. Thus, a typical warm-up time period of the erasing procedure and the estimated mobility relaxation time at 310 K are on the same order of magnitude. As we suspected, when analyzing the data shown in Figure 9, the photoenhancement of μ_H was indeed lost before the sample reached the 310 K erasing temperature, whereas it was still visible in p_H, due to the substantially longer relaxation time.

4 Discussion

4.1 Hall effect

The interpretation of the Hall effect measurements is one of the most heavily discussed topics in the field of HTS materials. The main problem is that p_H shows an unusual temperature dependence. In a classical metal, p_H is more or less temperature independent and closely matches the concentration of mobile charge carriers. In metallic YBCO [32], as well as in Bi-based [33] and Tl-based [34] compounds, p_H depends almost linearly on T above T_c. Thus, p_H calculated from the simple one-band formula $p_H = 1/R_H e$ cannot be directly identified as the density of charge carriers. On the other hand, the Hall angle $\tan\,\theta_H = \mu_H B$ in HTS materials uniformly obeys the empirical law [32–35]:

$$\cot\,\theta_H = \alpha T^2 + C, \tag{2}$$

where α and C are constants. The T^2-dependence indicates that the electron-electron (or, more generally, fermion-fermion) scattering mechanism. Such mechanism plays an important role in normal metals only at low temperatures, while in HTS is clearly dominant up to room temperature.

A great variety of models have been proposed to explain this remarkable equation (2) dependence in HTS samples (see, *e.g.*, Refs. [32,35] and references therein), but most of them are concerned with only one of the quantities, either p_H or μ_H and only the Luttinger-liquid model of Anderson [36] seems able to describe the temperature dependences of both quantities. Starting with the Anderson model, Jones *et al.* [35] have derived the temperature dependence of p_H in YBCO, which agrees well with our experimental observations in the temperature range from 150 to 310 K:

$$p_H \propto \cot\,\theta_H/\rho_{xx} \propto nT, \tag{3}$$

where n is the concentration of charge carriers. Thus, the *changes* of p_H and μ_H, observed at an arbitrarily fixed temperature, in fact measure the changes of the carrier concentration and the mobility, like in the conventional spherical one-band model. This consideration is crucial for the interpretation of our *in situ* Hall effect measurements and is strongly supported by the fact that δp_H and ΔT_c in our photodoping experiments show essentially the same dependence on the photodoping temperature (Fig. 7). Note that the good agreement extends down to 70 K, where the linear temperature variation of p_H (Eq. (3)) is not strictly obeyed. Apparently, both quantities measure the same physical parameter, *i.e.*, the change of the carrier concentration. Therefore, in the following discussion, we will use the terms carrier concentration n and mobility μ interchangeably with p_H and μ_H.

4.2 Influence of photodoping on carrier properties

At first, we will briefly summarize predictions that the different PPC models (outlined in Sect. 1) give for photodoping's impact on carrier properties. In the *charge transfer*

as well as in the *oxygen vacancy capture* model, photodoping should increase mainly the carrier concentration. For the mobility, if it is affected at all, one would expect its decrease rather than an increase since randomly distributed trapped electrons should introduce a certain amount of disorder in the material. In addition, the increasing number of charge carriers (holes) should increase the fermion-fermion scattering rate. This picture is consistent with the experimental results [32] that show that $\tan\theta_H$, taken at a fixed temperature, decreases with the increase of the oxygen content, indicating a slight decrease of μ_H as a function of the carrier density.

The *photoassisted oxygen-ordering* model gives a very special prediction, namely a close relationship between the photoinduced change of the carrier concentration and the mobility. In this model, electrons are not only trapped in the CuO chains but give rise to an increase of the length of chain segments. Thus, n is enhanced in two ways: first, electrons trapped in the chains result in mobile holes in the CuO_2 planes; second, the chains are lengthened, inducing an additional charge transfer from planes to chains. Injection of holes into planes by the chain-growth mechanism is less effective than any direct charge-transfer process, since only chain segments longer than 4 CuO units contribute to the carrier density [37]. However, the growth of the chains must have impact on the electronic and the crystal structure of the material, as well as on μ of the charge carriers. From general considerations, we expect that oxygen ordering should *increase* the carrier mobility since removing disorder from a system increases the average scattering time. However, in experiments of room-temperature aging of quenched YBCO samples, a decrease of μ_H was observed [6]. Admittedly, the analogy between the photoassisted oxygen ordering and oxygen ordering in quenched samples is limited. The photodoping starts with the sample in more-or-less equilibrium conditions and subsequently lowers the degree of thermally driven disorder, simultaneously removing the system from its initial thermodynamical equilibrium. This is in sharp contrast to the oxygen ordering, occurring in the quenched sample, which moves the system towards the intrinsic equilibrium state. Thus, despite apparent analogies (*e.g.*, the applicability of Eq. (1)), the results of room-temperature aging experiments cannot be directly taken as a model for photoassisted oxygen ordering.

The most striking of our experimental result is the markedly different time dependences of p_H and μ_H. This finding certainly cannot be explained by implementing exclusively the *oxygen-ordering* model since this model predicts a very close relationship between p_H and μ_H. In particular, the positive-to-negative change of the slope of $\mu_H(t)$ at high temperatures (Fig. 4) should have been somehow reflected in $p_H(t)$, which is obviously not the case. On the other hand, only *oxygen ordering* seems capable of giving a reasonable explanation for the increasing part of the mobility observed at all temperatures. Thus, our conclusion is that oxygen ordering takes place during the light illumination, but it enhances mainly μ and has only a limited effect on n.

The decreasing component of the mobility during a prolonged illumination μ_{dec} (Fig. 4) is an intriguing phenomenon. The behavior is observable only in the $T > 250$ K-range, where the thermal relaxation of PPC occurs in metallic YBCO [13]. This suggests that both effects must have a common physical origin, implying that PPC relaxation during the photoexcitation process manifests itself in the behavior of the mobility, long before it affects the carrier concentration (compare Figs. 3 and 4). The possible reason for this intriguing consequence is that the kinetics of oxygen ordering/disordering is strongly accelerated when the temperature approaches room temperature, due to the increasing diffusivity of oxygen [38], as it is indicated by the results shown in Figure 5. It appears that the thermal relaxation process gradually destroys the photoinduced ordering effects in the chains, simultaneously having only a limited influence on the carrier density, or it is overcompensated by an enhanced photogeneration of additional carriers. This would explain why, after long exposure times, μ_H falls below even its initial, undoped value, despite the fact that one would expect PPC relaxation to cancel only the photoinduced enhancement of μ. We observed this effect also in our photodoping/relaxation experiment (Fig. 10), so the assignment of the falling component of μ to the thermal PPC relaxation is a consistent interpretation of our data. However, μ_{dec} keeps decreasing even after 48 h of illumination (Fig. 4), while μ_H under dark conditions saturates within about 15 h (Fig. 10), indicating differences between relaxation processes with or without light exposure and again pointing to *photoassisted oxygen ordering* as a mechanism for enhancing mobility (see Sect. 4.3).

The main contribution to the enhancement of n originates from the photodoping mechanisms that have little or no influence on μ. The *charge transfer* and the *oxygen vacancy capture* mechanisms are the main candidates for such processes; however, other mechanisms, such as trapping of photoexcited electrons by impurities or in lattice distortions/grain boundaries may also play a role, as indicated in the relaxation studies discussed below. However, it is obvious from Figure 3 that the enhancement of n, being almost the same at all temperatures up to 200 K, rises substantially near room temperature, *i.e.*, in the same temperature region where μ_H exhibits its unusual behavior (Fig. 4) and the thermal PPC relaxation becomes important [13,14]. Thus, our data seems to indicate that the disordering processes observed in this temperature region favor the photogeneration of charge carriers *via* the charge transfer processes. Possibly, thermal disordering creates additional oxygen vacancies or other defects that may act as trapping centers for the photogenerated electrons.

4.3 PPC relaxation effects

The results presented in Section 3.3 indicate that, after the illumination is terminated, μ relaxes far more rapidly than n. The short PPC relaxation time (Fig. 10) clearly contradicts the results obtained in the room-temperature

aging experiments [6]. We point out again that the physical situation in both types of these experiments is quite different. In the room-temperature aging case, an oxygen-depleted YBCO sample is quenched from high temperatures to room temperature. Hence, at the beginning of the experiment, the sample is in a highly nonequilibrium state and relaxes back to equilibrium. In other words, room-temperature aging means a relaxation from a highly disordered state to a more ordered one. In the photodoping experiments, our sample is initially in an equilibrated state (at least near room temperature) with a certain amount of disorder due to thermal activation. Photoassisted oxygen ordering, as characterized by our measurements, partially reorders the system. When the illumination is terminated, the system relaxes toward a more disordered state, *i.e.*, in the opposite direction as compared to the room-temperature aging. In our opinion, the similarities between the two processes arise only from the fact that they are driven by movements of the same molecules, namely oxygen ions. On the other hand, the differences in kinetics are too obvious to expect the same experimental results in both cases. This conclusion applies also to the μ enhancement, attributed to oxygen ordering, despite the disagreement with the room-temperature aging experiments.

An even more intriguing result from our relaxation studies is the fact that μ_H falls below its initial, undoped value and stays constant for the remaining duration of our experiment (Fig. 10). From the Kohlrausch fits we learn that the theoretical saturation values of $\mu_H(t)/\mu_H(0)$ and $p_H(t)/p_H(0)$ are 0.99 and 1.03, respectively. Since $\Delta\sigma/\sigma \cong \Delta p_H/p_H + \Delta\mu_H/\mu_H$, one could expect for $t \to \infty$ a remaining conductivity enhancement of about 2%, suggesting that at 290 K, the PPC does not completely relax. The photoexcited state relaxes into a system that differs from the undoped one, *e.g.*, is characterized by a small fraction of photoexcited electrons trapped at 290 K. This may indicate that, besides the *charge transfer* and the *photoassisted oxygen-ordering* processes, additional mechanisms like electron trapping at grain boundaries or on lattice defects are involved in the PPC process. At 310 K, however, the PPC relaxation was always complete, and both $\rho_{xx}(t)$ and $\rho_{yx}(t)$ reached the values of the undoped material, regardless of the preceding history of the photodoping experiment. Hence, we believe that the photoinduced state, being still metastable at 290 K, can be erased at higher temperatures by strong thermal fluctuations. This observation, however, needs further experimental studies.

5 Conclusions

We have shown that the effect of prolonged white-light illumination on partially oxygen-depleted YBCO ($x \approx 6.5$, $T_{c,mid} \approx 52$ K) depends strongly on the temperature at which the photodoping experiment is performed. At low temperatures, photoexcitation leads to a state with enhanced carrier concentration *and* mobility. At temperatures above approximately 250 K, μ is reduced after long illumination times, whereas n is even more enhanced, compared to its value at low temperatures. Thus, photodoping at different temperatures generates in YBCO states with different electronic properties, resulting in different $\rho_{xx}(T)$ characteristics.

From the presented experimental results and their interpretation, we conclude that the *photoassisted oxygen-ordering* and *charge transfer* processes from CuO_2 planes to CuO chains are the main contributors to the PPC effect; however, their relative contributions are different and strongly depend on the temperature of the photodoping process. The *oxygen-ordering* mechanism is mainly responsible for the changes of μ, while the *charge transfer* acts on n. However, there is additional evidence from the relaxation data that other mechanisms, like trapping of electrons in lattice defects or at grain boundaries, give some contribution to PPC. We have shown also that the T_c enhancement due to photodoping is a function of the carrier concentration rather than of the mobility.

The relaxation of the photoexcited state has a different nature than the room-temperature aging of thermally quenched YBCO samples. In particular, μ relaxes far more rapidly after the termination of photodoping than after quenching the samples from high temperatures to room temperature. Moreover, the mobility saturates at a value below the undoped one, suggesting that photodoping leads to rearrangements of oxygen ions different than an abrupt change of temperature.

This work was supported by the Fonds zur Förderung der wissenschaftlichen Forschung, Austria, and the Air Force Office for Scientific Research grant F49620-94-1-0094, USA. Additional support from the Polish Government State Committee for Scientific Research grant 2P302 179 06 is also acknowledged.

References

1. V.I. Kudinov, A.I. Kirilyuk, N.M. Kreines, R. Laiho, E. Lähderanta, Phys. Lett. A **151**, 358 (1990).
2. V.I. Kudinov, I.L. Chaplygin, A.I. Kirilyuk, N.M. Kreines, R. Laiho, E. Lähderanta, Phys. Lett. A **157**, 290 (1991).
3. V.I. Kudinov, I.L. Chaplygin, A.I. Kirilyuk, N.M. Kreines, R. Laiho, E. Lähderanta, C. Ayache, Phys. Rev. B **47**, 9017 (1993).
4. V.I. Kudinov, Physica B **194-196**, 1963 (1994).
5. G. Nieva, E. Osquiguil, J. Guimpel, M. Maenhoudt, B. Wuyts, Y. Bruynseraede, M.B. Maple, I.K. Schuller, Appl. Phys. Lett. **60**, 2159 (1992).
6. E. Osquiguil, M. Maenhoudt, B. Wuyts, Y. Bruynseraede, D. Lederman, G. Nieva, J. Guimpel, I.K. Schuller, J. Alloys Comp. **195**, 667 (1993).
7. E. Osquiguil, M. Maenhoudt, B. Wuyts, Y. Bruynseraede, D. Lederman, I.K. Schuller, Phys. Rev. B **49**, 3675 (1994).
8. K. Tanabe, S. Kubo, F. Hosseini Teherani, H. Asano, M. Suzuki, Jpn J. Appl. Phys. **32**, L264 (1993).
9. K. Tanabe, S. Kubo, F. Hosseini Teherani, H. Asano, M. Suzuki, Phys. Rev. Lett. **72**, 1537 (1994).

10. K. Kawamoto, I. Hirabayashi, Phys. Rev. B **49**, 3655 (1994).
11. D. Lederman, J. Hasen, I.K. Schuller, V. Osquiguil, Y. Bruynseraede, Appl. Phys. Lett. **64**, 652 (1994).
12. W. Göb, W. Lang, W. Markowitsch, V. Schlosser, W. Kula, R. Sobolewski, Solid State Commun. **96**, 431 (1995).
13. W. Markowitsch, C. Stockinger, W. Göb, W. Lang, W. Kula, R. Sobolewski, Physica C **265**, 187 (1996).
14. V.I. Kudinov, A.I. Kirilyuk, N.M. Kreines, JETP Lett. **56**, 102 (1992).
15. K. Tanabe, S. Karimoto, S. Kubo, K. Tsuru, M. Suzuki, Phys. Rev. B **52**, 13152 (1995).
16. H. Szymczak, M. Baran, S.L. Gnatchenko, R. Szymczak, Y.F. Chen, Z.G. Ivanov, L.-G. Johansson, Europhys. Lett. **35**, 451 (1996).
17. R.P. Gupta, M. Gupta, Phys. Rev. B **44**, 2739 (1991).
18. P.K. Gallagher, Adv. Ceram. Mater. **2**, 632 (1987).
19. J.D. Jorgensen, M.A. Beno, D.G. Hinks, L. Soderholm, K.J. Volin, R.L. Hitterman, J.D. Grace, I.K. Schuller, C.U. Segre, K. Zhang, M.S. Kleefisch, Phys. Rev. B **36**, 3608 (1987).
20. B.W. Veal, A.P. Paulikas, Physica C **184**, 321 (1991).
21. C. Ayache, I.L. Chaplygin, A.I. Kirilyuk, N.M. Kreines, V.I. Kudinov, Solid State Commun. **81**, 41 (1992).
22. S.L. Bud'ko, H.H. Feng, M.F. Davis, J.C. Wolfe, P.H. Hor, Phys. Rev. B **48**, 16707 (1993).
23. S.L. Cooper, D. Reznik, A. Kotz, M.A. Karlow, R. Liu, M.V. Klein, W.C. Lee, J. Giapintzakis, D.M. Ginsberg, B.W. Veal, A.P. Paulikas, Phys. Rev. B **47**, 8233 (1993).
24. B.W. Veal, A.P. Paulikas, H. You, H. Shi, Y. Fang, J.W. Downey, Phys. Rev. B **42**, 6305 (1990).
25. J.-P. Locquet, J. Vanacken, B. Wuyts, Y. Bruynseraede, K. Zhang, I.K. Schuller, Europhys. Lett. **7**, 469 (1988).
26. J. Hasen, D. Lederman, I.K. Schuller, V.I. Kudinov, M. Maenhoudt, Y. Bruynseraede, Phys. Rev. B **51**, 1342 (1995).
27. N.M. Kreines, V.I. Kudinov, Mod. Phys. Lett. B **6**, 289 (1992).
28. W. Markowitsch, C. Stockinger, W. Lang, W. Kula, R. Sobolewski, *Spectroscopic Studies of Superconductors*, edited by I. Bozovic, D. van der Marel (SPIE, Bellingham, WA, 1996), vol. **2696**, part B, pp. 617-626.
29. R. Sobolewski, L. Shi, T. Gong, W. Xiong, Y. Kostoulas, P.M. Fauchet, *High-Temperature Superconducting Detectors: Bolometric and Nonbolometric*, edited by M. Nahum, J.-C. Villegier (SPIE, Bellingham, WA, 1994), Vol. **2159**, pp. 110-120.
30. W. Kula, W. Xiong, R. Sobolewski, J. Talvacchio, IEEE Trans. Appl. Supercond. **5**, 1177 (1995).
31. Y.J. Uemura, G.M. Luke, B.J. Sternlieb, J.H. Brewer, J.F. Carolan, W.N. Hardy, R. Kadono, J.R. Kempton, R.F. Kiefl, S.R. Kreitzman, P. Mulhern, T.M. Riseman, D.L. Williams, B.X. Yang, S. Uchida, H. Takagi, J. Gopalakrishnan, A.W. Sleight, M.A. Subramanian, C.L. Chien, M.Z. Cieplak, G. Xiao, V.Y. Lee, B.W. Statt, C.E. Stronach, W.J. Kossler, X.H. Yu, Phys. Rev. Lett. **62**, 2317 (1989).
32. B. Wuyts, E. Osquiguil, M. Maenhoudt, S. Libbrecht, Z.X. Gao, V. Bruynseraede, Phys. Rev. B **47**, 5512 (1993).
33. W. Lang, G. Heine, W. Kula, R. Sobolewski, Phys. Rev. B **51**, 9180 (1995).
34. N.P. Ong, *Physical Properties of High Temperature Superconductors II*, edited by D.M. Ginsberg (World Scientific, Singapore, 1990), p. 469.
35. E.C. Jones, D.K. Christen, J.R. Thompson, R. Feenstra, S. Zhu, D.H. Lowndes, J.M. Phillips, M.P. Siegal, J.D. Budai, Phys. Rev. B **47**, 8986 (1993).
36. P.W. Anderson, Phys. Rev. Lett. **67**, 2092 (1991).
37. G.V. Uimin, V.F. Gantmakher, A.M. Neminsky, L.A. Novomlinsky, D.V. Shovkun, P. Brüll, Physica C **192**, 481 (1992).
38. S.J. Rothman, J.L. Routbort, J.E. Bakar, Phys. Rev. B **40**, 8852 (1989).